Local structural motifs in a quenched model monatomic liquid

Randall A. LaViolette* and David M. Stump†
Idaho National Engineering Laboratory, P.O. Box 1625, Idaho Falls, Idaho 83415-2208
(Received 4 February 1994)

Amorphous packings have been generated from steepest-descent quenches applied to a monatomic liquid simulated by molecular dynamics. The model for the interatomic forces employed here provides both liquids and solids with a mean coordination as low as seven at low densities as well as the close-packed configurations with a mean coordination of twelve at higher densities. The low-coordination packings generated from the low-density liquid contain microcrystallites with a simple hexagonal structure which, with increasing density, are eventually suppressed in favor of microcrystallites with a body-centered-cubic (bcc) structure. The abrupt growth of the bcc microcrystallites occurs at densities well below the density for the hexagonal-bcc crystal transition at zero temperature and constant volume. The high-coordination packings quenched from the high-density liquid contain truly amorphous clusters which are neither crystalline nor icosahedral, but share attributes of both. The first result shows that microcrystalline clusters can be important structural elements of even simple amorphous substances. The second result resolves the conflicting claims concerning the abundance or scarcity of icosahedra in the densest amorphous substances. Both of these results challenge widely held pictures of simple amorphous substances.

I. INTRODUCTION

This paper is devoted to the elucidation of the local microscopic structural motifs found in mechanically stable amorphous packings of a simple monatomic model substance. The subject has a long history, in part due to the early appreciation that its study is fundamental in the theory of glasses, and also in part due to the simplicity of the interactions in these substances. On the other hand, the noncovalent monatomic substances represent the extreme among glass-forming substances, in that they are the most difficult to quench into glasses. An explanation for this is that the nuclei required for spontaneous crystallization can be microscopically small, of perhaps only a few atoms, and therefore even a mild density fluctuation might generate critical nuclei. Therefore, Frank and others have argued that the local structural motifs in monatomic metals, for example, should be other than crystalline.[1] Consequently, the idea that crystalline local order should prevail in simple amorphous deposits has been explicitly dismissed by many experts.[2,3] Instead, the noncrystalline icosahedron has been offered as a candidate for the local structure of dense metallic or simple glasses because the mean coordination in these substances is typically near 12 and because the icosahedron possesses the lowest energy among isolated 12-coordination cluster for a wide variety of models.[1–7]

The suggestion that the icosahedron is the predominant local structural motif in simple dense amorphous substances has been pursued mostly in theoretical studies, partly due to the difficulty of making the glasses and to the difficulty of analyzing such small structural features.[8] Although the majority report among researchers in the USA and Japan apparently favors icosahedra in amorphous packings of simple close-packed substances, objections have been raised on two different grounds. One is direct and empirical: Serious efforts by some researchers to identify icosahedra in dense glasses generated by computer simulation of monatomic substances with simple models for the interactions have found icosahedra to be scarce, in contrast to the large populations anticipated by theory.[9–11] One recent effort in computer simulations of glasses has attempted to increase the population of icosahedra by devising a special model for the interatomic forces, which specifically favors them, and consequently reports abundant icosahedra in the amorphous packings quenched from the computer-simulated liquid.[12] The other objection is indirect, pressed only by analogy to the topological-constraint theory of covalent (network) glass formers.[13] In this theory, an analysis of the meaning of glass formation in *configuration* space suggests that the local order is much higher than suggested by the alternative and widely held continuous-random-network model. The constraint theory leads to the argument that in some cases the local order of the network glass quenched from the liquid is essentially that of the high-temperature crystal phase at that density; thus for amorphous quartz at atmospheric pressures, for example, the local order should consist of cristobalite crystallites.[14,15] The constraint theory for network glasses has not been developed for metallic or other simple glasses. Nevertheless, an argument has been offered by analogy that insofar as microcrystalline order appears in network glasses, then perhaps it might be prominent in metallic glasses as well, even though critical nuclei for crystallization are also microscopic.[16] In view of the direct observations cited above, this analogy deserves further exploration. Therefore, the amorphous packings of a model substance will be examined not only for the presence of icosahedra and other structures, which minimize cluster energy, but also for the presence of microcrystalline clusters.

The study of local order in the close-packed amor-

phous packings of substances with a Van der Waals–like interaction (of which the Lennard-Jones model is a famous example) has proven to require some care because the various structures of high coordination can be difficult to distinguish. For example, although the perfect icosahedron and the perfect face-centered-cubic crystallite are readily distinguished, only a little distortion is necessary to transform one arrangement into the other. The techniques applied in Sec. VI below provide one solution to this problem. However, a potentially more revealing alternative is simply to examine amorphous packings which are more loosely packed. It is possible in such cases that the varieties of local order might be more easily distinguished. A simple model, which provides lower-coordination amorphous packings, is the *hx* pair potential, described in detail in Sec. II below. Although the *hx* model shares several qualitative features with the Lennard-Jones model, the latter reaches the global energy minimum with the hexagonal close-packed lattice,[17] while the *hx* model finds it with a simple hexagonal lattice. Therefore, the *hx* model is able to generate low-coordination amorphous packings at low densities (and positive pressures) as well as the usual high-coordination packings at high densities.

Following the review of the *hx* model below, a brief description of the computational methods employed here is provided in Sec. III. Section IV contains some results for the local amorphous packings over the whole density range. Section V contains results for the local structure of the low-coordination packings. Section VI contains the results for the high-coordination packings. This paper concludes in Sec. VII with a discussion of the significance of these results.

II. REVIEW OF THE *hx* MODEL

The potential energy $u(r)$ between a pair of *hx* particles separated by the distance r is given by

$$u(r)=1.914\,166\,098(r^{-12}-r^{3})\exp[1/(r-2)], \quad r<2 , \tag{1}$$

$$u(r)=0, \quad u'(r)=0, \quad u''(r)=0, \quad u'''(r)=0,\ldots, \quad r\geq 2 .$$

The distance r is written in reduced units so that the diameter, defined by the first instance of $u=0$, is unity. The energy is also written in reduced units, so that $u=-1$ at the minimum.

The *hx* model[18] is so called because the simple hexagonal lattice, at the density $n=0.8895$ and c/a ratio of 0.9092, provides the global energy minimum, with a per-particle energy of -7.3807. It was employed here for the diversity of structures it produces. At zero temperature and constant volume, the stable crystals range from simple hexagonal (with varying c/a near unity) to body centered cubic to hexagonal close packed to face centered cubic as the density increases. Table I indicates the constant-volume transition densities.[19] This ability of *hx* to support his diversity of low-coordination and high-coordination structures is apparently unique among simple pair-potential models. For example, the Lennard-Jones pair potential [$u(r)=4(r^{-12}-r^{-6})$ in our units],

TABLE I. Transition densities for the zero-temperature crystalline phases of *hx*. The simple hexagonal phase is denoted by hex, body-centered cubic is bcc, hexagonal close packed is hcp, and face centered cubic is fcc.

Transition density	Transition type
1.24	hex→bcc
1.29	bcc→hcp
1.34	hcp→fcc

and its truncated variants produce only high-coordination close-packed crystals at zero temperature for the same density range, even at densities for which the crystals would be under severe tension. Of course, the Lennard-Jones potential was intended to model real substances, but no such claim is made for *hx*; indeed, the only elements with a simple hexagonal structure (and comparable c/a ratios) are high-pressure forms of carbon and silicon.[20]

Figure 1 sketches the *hx* and the Lennard-Jones model together, showing that the repulsions are much softer, the minimum is much farther, and the attractive well is much wider in the *hx* model than in the Lennard-Jones model. These features account for the former's ability to sustain the low-coordination structures at low densities. On the other hand, at sufficiently high densities, *hx* behaves in a fashion similar to the Lennard-Jones model and its many variants, which sustain high-coordination structures. Furthermore, *hx* shares with the Lennard-Jones model the habit of obtaining the global minimum

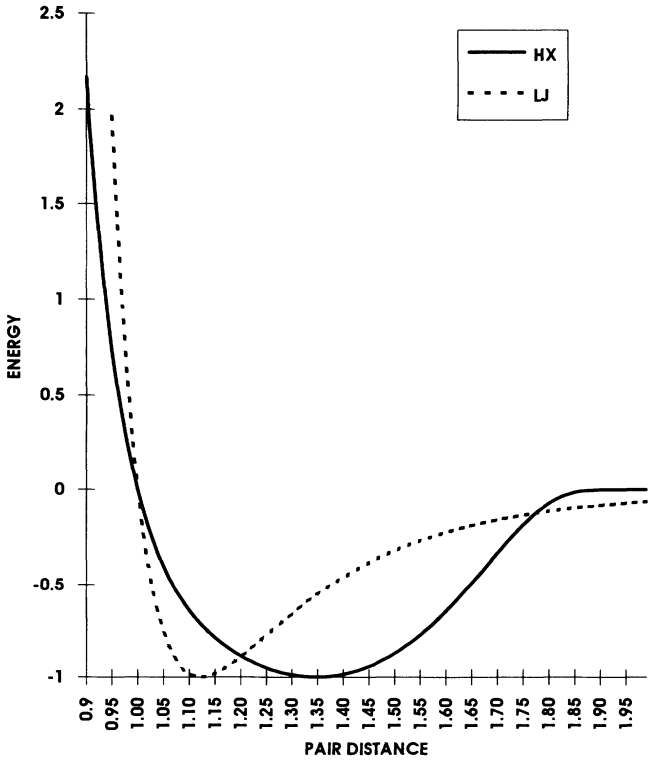

FIG. 1. Pair-potential energy for *hx* and Lennard-Jones models, respectively, in reduced units.

energy of the isolated 12-coordination cluster with the icosahedron, which for *hx* has (counting all 13 particles) an energy of -41.802 and a radius of 1.299 26. This energy is well below the energy of the cluster with either the face-centered-cubic or hexagonal close-packed lattice, which for either is -36.062 with lattice parameters corresponding to $n=0.793$.

III. COMPUTATIONAL PROCEDURES

This study was carried out by first simulating a liquid of *hx* particles with molecular dynamics, then quenching that liquid at several intervals, and finally by analyzing the structural details of the collection of quenched amorphous packings. These procedures are described below.

Molecular dynamics was applied to a system of 500 *hx* particles in a cubic box subject to periodic boundary conditions in order to simulate a liquid at between three and five times it s melting temperature. For each density, the constant-volume equations of motion were solved with the fifth-order Gear-Nordsieck algorithm,[21] with time steps (between 0.001 and 0.005 in reduced units) adjusted to maintain energy conservation to at least five digits for the duration of the runs. "Double precision" was maintained throughout the calculation. Following equilibration runs of between 5000 and 10 000 steps, runs during which the quenches were taken ran typically for 10^5 steps. At intervals of at least 2000 steps in a molecular-dynamics run, the 500-particle configuration was selected and quenched at constant volume with an efficient algorithm which alternates between steepest-descent and quasi-Newton procedures.[22] This implementation guarantees that the quench instantaneously removes all the kinetic energy and moves the configuration to the nearest local potential-energy minimum without the possibility of annealing. The amorphous packings must always be mechanically stable, which was randomly checked by examining the eigenvalues of the dynamical (or "force constant") matrix. It happens frequently in quenches generated either by simple but less efficient steepest-descent procedures or by procedures that do not employ at least the forces (such as setting $T=0$ in a canonical-ensemble Monte Carlo calculation) that the quench is terminated well before the packing reaches a genuine local potential energy minimum. The algorithm employed here, on the other hand, almost never fails to produce a packing at a genuine minimum. However, both the algorithm itself and the subsequent check of the dynamical matrix severely limit the system size; consequently, quenches of a much larger system were not attempted here.

Between 24 and 78 stable packings were collected from the simulated liquid for each density. The ensemble of stable amorphous packings quenched from the liquid is called by Stillinger the "inherent structure" of the liquid at that density.[23] It has been established that the inherent structure of simple monatomic liquids is independent of temperature for temperatures at or above the melting temperature; in particular, temperature independence was established for a liquid of *hx* particles.[24]

The analysis of the local structure in the amorphous packings requires an unbiased and unambiguous method for identifying nearest neighbors. This is done here by

TABLE II. Attributes of the inherent structure of *hx* at various densities. The relative uncertainties associated with the energy are less than 1% for densities below 1.57; thereafter the uncertainties rise up to 12% for the highest density. For the pressure, the relative uncertainties typically lie between 2% and 5% , except near zero pressure, where they rise up to 20%. No estimate of the uncertainty was made for r_{NN}, which was found by the three-point Lagrange interpolation for the interval in $g(r)$ around the minimum between the first and second peaks. For the mean coordination the absolute uncertainty is 1. All of these values were taken at zero temperature.

Density	Number of quenches	Energy	Pressure	r_{NN}	Mean coordination
0.7800	49	−6.66	−1.10	1.293 485	6.7
0.8400	24	−6.76	−0.67	1.265 502	6.9
0.8750	74	−6.80	−0.29	1.240 522	6.9
0.8895	54	−6.80	−0.09	1.229 910	6.9
0.9050	74	−6.81	0.12	1.225 462	6.9
0.9500	74	−6.79	0.80	1.217 249	7.3
1.0000	58	−6.73	1.6	1.216 266	7.9
1.0500	44	−6.63	2.4	1.217 785	8.5
1.1327	32	−6.41	4.0	1.210 801	9.3
1.1762	36	−6.27	4.9	1.209 631	9.7
1.2198	78	−6.10	5.8	1.212 166	10
1.2672	60	−5.92	6.8	1.215 535	11
1.3200	45	−5.40	8.4	1.220 395	11
1.4000	52	−5.31	12	1.218 336	11
1.4500	65	−4.98	16	1.216 921	12
1.5200	50	−4.40	23	1.206 415	12
1.5710	39	−3.88	29	1.205 646	12
1.6200	50	−3.28	37	1.184 981	12
1.9726	40	4.61	132	1.091 842	12

examining the pair distribution function, presented in the next two sections. The first peak of the pair distribution function represents the clustering of the nearest neighbors around a given particle; therefore, the minimum r_{NN} between the first and second peaks of the pair distribution function provides a statistically and physically significant criterion for selecting nearest neighbors. All particles whose centers are within r_{NN} of the central particle are regarded as its nearest neighbors. The radius r_{NN} is sensitive to the density of the packings, as indicated in Table II (cf. Sec. IV below).

With r_{NN} in hand for each density, every particle in every inherent structure is classified according to its coordination number. Furthermore, the arrangement of the nearest neighbors in each cluster can be studied in detail. For example, the principal axes, the distribution of pair distances, and the distribution of angles between the nearest neighbors, can be calculated for each of the thousands of clusters found in the inherent structure. Of these measurements, the last provides the most insight into the local structure of amorphous packings. The following three sections contain the results of these calculations.

IV. RESULTS FOR THE WHOLE DENSITY RANGE

At each of the densities listed in Table II, the quenched amorphous packings are collected and assayed for their properties at constant volume and zero temperature. The energy and pressure are tabulated in Table II. Interpolation suggests that the energy minimum for the inherent structure is found at about $n=0.915$, near the corresponding minimum ($n=0.8895$, cf. Sec. II) for the crystal energy. The per-particle energy of the inherent structure at this density is -6.82, substantially above the energy of the underlying simple hexagonal crystal at this density of -7.37 (with $c/a=0.9165$). Although the mean coordination is about seven in the inherent structure compared to exactly eight in the simple hexagonal crystal, the mean bond energy in the inherent structure is actually about 5% lower than that in the crystal. The energy variation with density is otherwise unremarkable, providing little insight into the local structure of the amorphous packings. Much the same can be said for the equation of state, which also reveals little about structure. For example, no sensitivity to the phase transitions in the underlying zero-temperature crystal is found in either the energy or the pressure. Figure 2 shows that the enthalpy (per particle) for the inherent structure increases monotonically and unremarkably with increasing density.

The order parameter usually employed in the study of liquids and amorphous solids is the pair distribution function $g(r)$, and is sketched for various densities in Fig. 3. Although the variation due to density is more interesting, it is also quite gradual. At the higher densities, $g(r)$ closely resembles the pair distribution function, which would be found for an amorphous packing of Lennard-Jones particles, and like those found experimentally for amorphous films of monatomic metals. At the lower densities, $g(r)$ at first appears radically different, but closer inspection shows that essential similarities remain. The second and third peaks, for example, still correspond to the split second-neighbor distribution which is characteristic of all monatomic amorphous packings. In every case the order is short ranged, assuring that the packings are indeed amorphous, for $g(r)$ flattens out to unity beyond the fifth-nearest neighbors, as would be found for a uniform fluid.

The nearest-neighbor distance r_{NN} was determined for each density from the corresponding-pair distribution, as described above in Sec. III, and is also listed in Table II. The mean coordination number $\langle NN \rangle$ is listed in Table II and displayed in Fig. 2. For low densities, $\langle NN \rangle$ ranges between about seven and ten, gradually increasing to twelve for the higher densities. The variation is for the most part a gradual monotonic increase with density. Again, no sensitivity to the phase transitions in the underlying zero-temperature crystal is evident. The distribution of coordination numbers is roughly a normal distribution with a dispersion of unity.

There is little in these conventional measures to suggest that the amorphous packings possess any unusual or otherwise interesting structural features. The usual order parameter $g(r)$ provides a standard by which most mod-

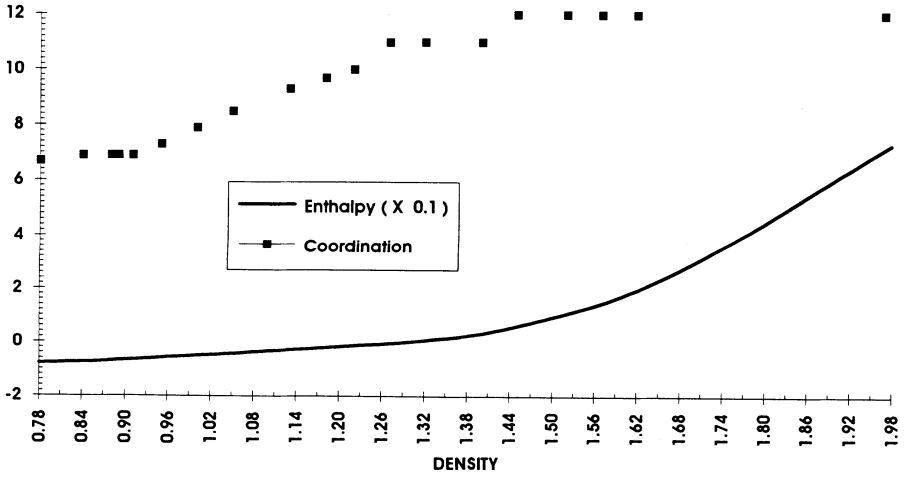

FIG. 2. Mean coordination number and enthalpy ($U/N + p/n$) for the inherent structure at zero temperature as a function of density.

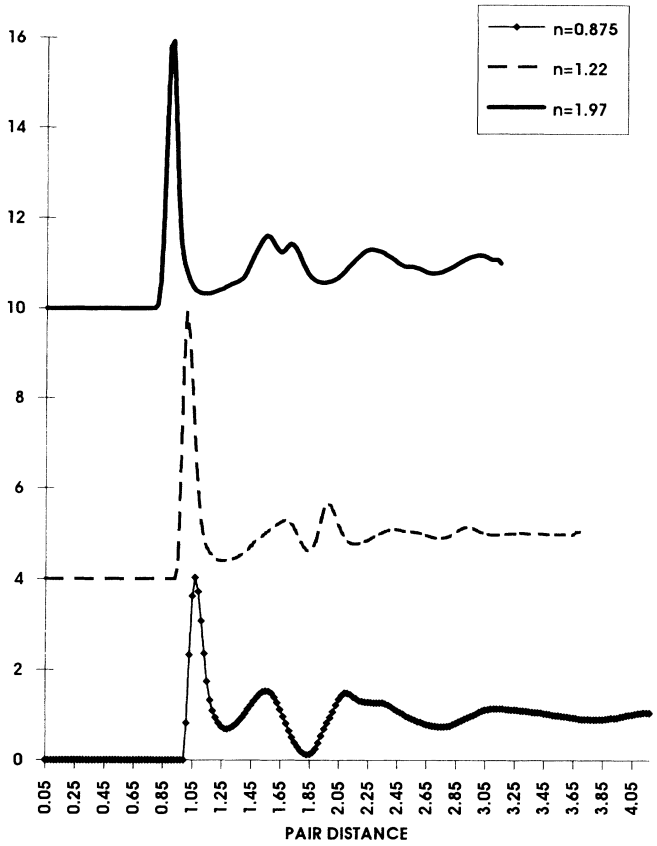

FIG. 3. Pair-distribution function of the inherent structure at three densities.

els and theories judged, yet here does little more than reflect the fact that the coordination changes with density and that the packings possess only short-ranged order. Therefore, the next two sections are devoted to a more detailed analysis of the packings in order to elucidate their local structure, first for the low-density range, and then for the high-density range.

V. LOCAL STRUCTURE OF THE LOW-DENSITY PACKINGS

Eight-coordination clusters are the focus of this investigation in the low-density range ($0.78 \leq n \leq 1.27$) because first, the two underlying crystal structures in this range (simple hexagonal and body centered cubic) are eight coordination, and, second, because eight-coordination clusters are abundant throughout this density range. Among the many possible eight-coordination arrangements, only three structure types are considered: simple hexagonal (hex), body-centered cubic (bcc), and the irregular structure (hxg), which provides the global energy minimum for the eight-coordination cluster in the ideal gas. Further inspection shows that the hxg cluster is a slightly distorted fragment of the icosahedron, and is displayed in perspective in Fig. 4. The idea that all clusters are either hex, bcc, or hxg clusters is based primarily upon inspection, and secondarily by reasoning that each of these structures is so different from the other that,

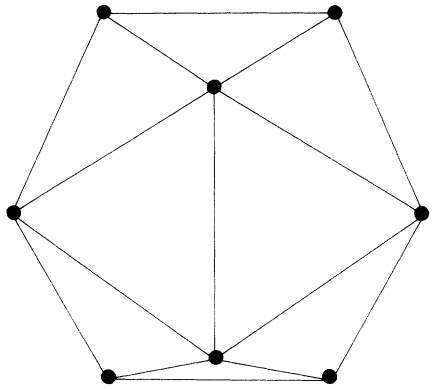

FIG. 4. Minimum-energy structure of the isolated eight-coordination cluster of hx particles. The particle nearest the center of mass is not shown. The structure, referred to as hxg in the text, is a slightly distorted fragment of an icosahedron.

loosely speaking, they might reasonably be expected to span the set of all eight-coordination structures, which could be encountered in the low-density inherent structure.

The analysis of the local structure of the low-density packings then becomes the calculation of the composition of the hex, bcc, and hxg structures among the eight-coordination clusters. This calculation depends on the choice of a property P of all the clusters so that for each density

$$P = \sum_{m=\{\text{hex,bcc,hxg}\}} c_m P_m \ , \tag{2}$$

where c_m is the concentration of one of the structures, and P_m is the mean value of the property for that structure. Some of the properties that were considered, tried, and rejected were the energy, the principal axes of the cluster, and the cluster pair distribution. The difficulty with each of these properties is their poor selectivity; these properties are each too insensitive to the differences between the three structure types.

One property for which the differences between the structure types are striking is the angle between pairs of the eight particles on the perimeter of the cluster, with the center of mass as the vertex. The angles and their populations for each of the structure types is tabulated in the first two columns of Table III. For example, only the

TABLE III. Parameters for the normalized Gaussian functions ϕ employed in Eq. (3). Unshifted angles θ_k are given in degrees. The frequency a_k of the angles multiplied by the number of distinct angles in each eight-coordinated cluster gives the respective angle populations. Both the empirical multipliers b_k and the shift to θ_k (also given in degrees) were determined by examining the effect of random displacements on the structure type.

	θ_k	a_k^*28	b_k	Shifts
bcc	71,109,180	12,12,4	1,1,2	0,0,−5
hex	60,90,120,180	6,12,6,4	2,1,2,2	0,0,0,−5
hxg	58,65,67,83,93,110, 122,143,145,159	2,4,4,4,1, 2,4,4,2,1	1,1,1,1,1, 1,2,1,1,1	0

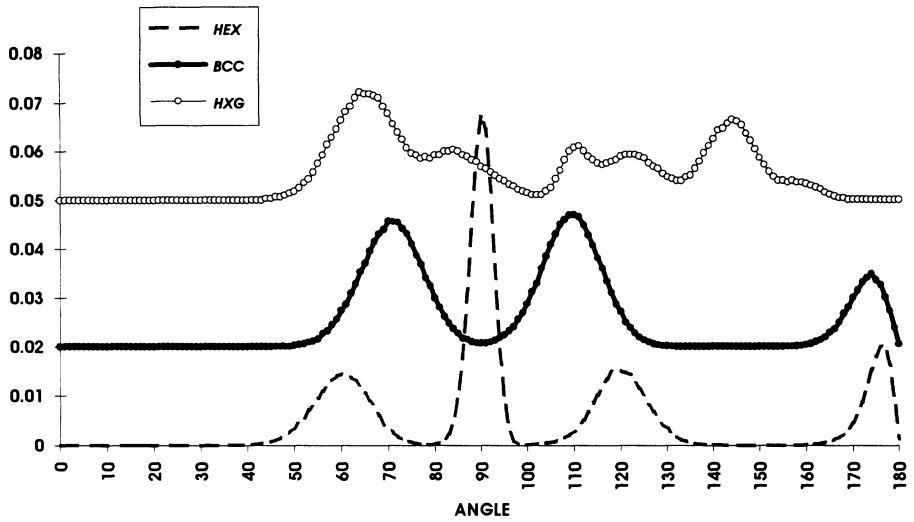

FIG. 5. Angle distribution for each of the eight-coordination structure types. Each of the angle distributions have been broadened with a Gaussian spreading function (see Table III).

hex structure type possesses perpendicular angles. Furthermore, although both hex and bcc types possess a center of inversion, hxg does not, and consequently it possesses no angles of 180°. Each of the angle distributions is sufficiently distinct that it makes to attempt a fit as outlined in Eq. (2), where P is the angle distribution sampled from all the eight-coordination clusters in the inherent structure. Another advantage offered by the angle distribution is that it appears relatively insensitive to distortions, unlike the pair distribution, for example. In order to assess in advance the effect of distortions upon the angle distributions for each of the structure types, each type had each of its eight perimeter particles randomly displaced (taken from the normal distribution) about 5000 times. The resulting distributions are shown in Fig. 5 for one choice of dispersion ($\sigma=0.15$) in the normal distribution of displacements. One noticeable effect on the crystalline structure types (hex and bcc) is the displacement of the peak at 180°. For hxg, several of the peaks combine into a single broad peak. The trends for the peak positions and widths portrayed in Fig. 5 are maintained for a wide range of values of the dispersion. These trends are incorporated into a fitting scheme designed to determine the c_m, the concentration of the structure type m in the inherent structure, as follows. First, the P_m in Eq. (2) is written as

$$P_m(\sigma)=\sum_{k=1}^{m_\theta} a_k \phi(\theta_k, b_k \sigma) , \tag{3}$$

where m_θ is the number of angles in type m, ϕ is the Gaussian function centered at θ and normalized over the range of angles $0 \le \theta \le \pi$, a_k is the fraction of angles in the distribution for type m, and b_k is a multiplier of dispersion σ deduced from the trends portrayed in Fig. 5. Table III lists the θ_k, a_k, and b_k for each structure type. The θ_k used in ϕ are shifted by the amount listed in the last column in Table III. With only one varying parameter (σ) for each of the structure types, the fitting procedure employs a search in the three-dimensional σ space via simulated annealing. For each guess of $\{\sigma_{\text{hex}}, \sigma_{\text{bcc}}, \sigma_{\text{hxg}}\}$, Eq. (2) was solved for the c_m with the singular-values decomposition (SVD) linear least-squares algorithm.[25] The search in σ space continued until the χ^2 produced by the SVD fit was at a global minimum; χ^2 was found to be between one and two at the minimum in all cases considered. At the beginning of the minimization procedure, the population of the hxg icosahedral-like clusters always appears dominant, but as the minimization proceeds and the fit is refined, the population of the

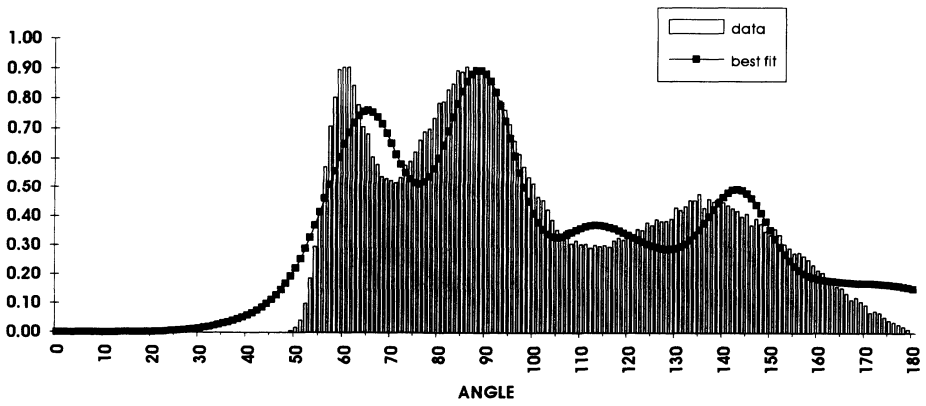

FIG. 6. Comparison of the fit of Eq. (2) with the measured angle distribution of eight-coordination particles for the inherent structure at $n=0.905$. The distributions have been normalized for angles on the interval $[0,\pi]$; angles in degrees are shown on the abscissa for convenience.

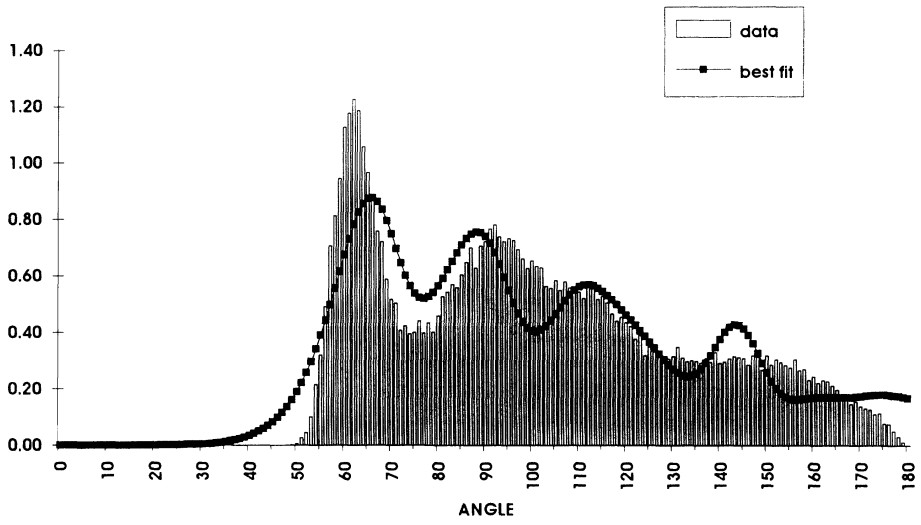

FIG. 7. Comparison of the fit of Eq. (2) with the measured angle distribution of eight-coordination particles for the inherent structure at $n=1.133$. The distributions have been normalized for angles on the interval $[0,\pi]$; angles in degrees are shown on the abscissa for convenience.

crystallization-like clusters hex and bcc always increases.

Typical results for the fit of the angle distribution are shown in Figs. 6 and 7, which also present the computed angle distribution. Even apart from the fitting procedure, comparison of Figs. 6 and 7 shows that clusters with perpendicular angles are most important at the lower densities; these clusters must be the hex structure types (cf. Fig. 5). Although the fits are far from perfect, they are good considering that only three parameters are varied. Presumably even better fits could also be had by varying the θ_k and b_k for each of the structure types, but the fits obtained with only three independent parameters are sufficient to measure the changes in composition of the inherent structure with increasing density. Furthermore, the deviations between the fits and the computed distribution are almost entirely due to an overestimate of the contribution of the hxg icosahedral-like structure types. Therefore, conclusions about the importance of crystalline-like structure types are likely to be strengthened by improvements in the fit. For now, we are content to perform a qualitative rather than a precise quantitative assay of the cluster types in the deposits. Finally, we note that when the same procedure is applied to a fluid, using the nearest-neighbor distance determined by its $g(r)$, the distribution is essentially featureless.

TABLE IV. Populations of structure types among eight-coordinated clusters. The rows do not all add up to 100% because of rounding errors.

Density	hex	bcc	hxg
0.7800	30%	0%	70%
0.8400	30%	0%	70%
0.8750	40%	0%	60%
0.8895	40%	0%	60%
0.9050	40%	0%	60%
0.9500	40%	5%	50%
1.0000	40%	10%	50%
1.0500	40%	20%	40%
1.1327	20%	40%	40%
1.2198	10%	60%	30%
1.2672	10%	60%	30%

Table IV contains the results for the composition in the low-density range $0.78 \le n < 1.27$, which are also displayed in Fig. 8. This is the main result for this section. The hxg clusters are in the majority for most of the range. For the lowest density, a substantial presence of hex clusters is found, with a maximum near $n=0.92$, where about 45% of the clusters are hex. This maximum is achieved just before the abrupt growth of bcc clusters, which begins in the interval $0.95 < n < 1.00$, below which the population of bcc clusters is negligible. The population of bcc clusters grows with increasing density at the expense of first hex then hxg clusters at densities well below that of the transition between the simple hexagonal and the bcc phases in the corresponding zero-temperature crystal (cf. Table I). For densities above $n=1.1$, bcc clusters dominate the eight-coordination cluster population. Again, a precise assay is neither intended nor achieved here, but the qualitative picture is clear: A transition occurs between the crystalline-like clusters, and crystalline-like clusters are always important, even though icosahedral-like clusters are also found at all densities.

The temperature independence of the inherent structure is expected to break down as the liquid is supercooled. As a test, the liquid was supercooled at two densities ($n=0.905$ and 1.133) without nucleation of a crystal phase to about one-fourth their respective freezing temperatures. Even at such low temperatures, however, the pair-distribution function and the results presented above in Fig. 8 and Table IV, respectively, remain essentially unchanged.

VI. LOCAL STRUCTURE OF THE HIGH-DENSITY PACKINGS

Twelve-coordination clusters are the focus of the investigation in the high-density range ($1.32 \le n \le 1.97$), in which they are abundant. As discussed elsewhere, the

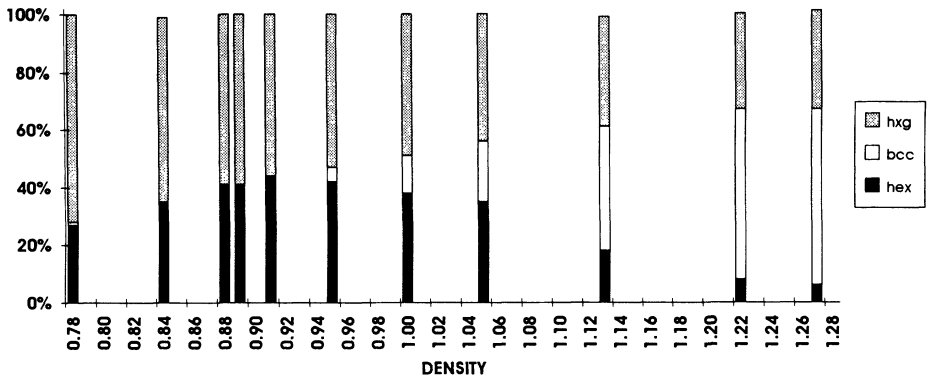

FIG. 8. Relative population of the three eight-coordination structure types in the inherent structure for various densities (see Table IV).

two principal structure types are the icosahedron (ico) and the two closed-packed crystal structures, hexagonal closed packed hcp and face centered cubic fcc (together denoted as closed-packed crystal, cpc). The icosahedron is the minimum-energy structure for the isolated 12-coordination cluster; the corresponding zero-temperature crystal phase is face centered cubic for $n > 1.34$ (cf. Table I). Once again the angle distribution of the 12-coordination clusters in the inherent structures are compared with the angle distributions of the now two structure types, ico and cpc. The comparison is facilitated by the observation that the icosahedron possesses no perpendicular angles but only angles of 63°, 114°, and 180°, while the fcc and the hcp crystallites each possess exactly 12 perpendicular angles out of the 66 distinct angles, besides angles of 60°, 120°, and 180° for the fcc and 60°, 109°, 120°, 146°, and 180° for the hcp crystallite. Figure 9 shows the angle distribution for the inherent structure at $n = 1.45$, typical for this density range. First, it is quite different from the angle distributions shown for the low-density range in Figs. 6 and 7. Second, the peak about the perpendicular angle is quite sharp, thereby permitting a statistical identification of the perpendicular angle as follows: all angles that lie between the minima on either side of the peak about 90° shall be regarded as a perpendicular angle. This definition provides a natural criterion for selecting perpendicular angles, and therefore structure types. It avoids the arbitrary cutoffs, which some other procedures must invoke when discriminating between icosahedral and close-packed structures, including the one previously employed by this author. Therefore, a cluster is here regarded as icosahedral only if it contains no perpendicular angles as just defined. On the other hand, a cluster is regarded as cpc only if it contains exactly 12 perpendicular angles. Clusters that contain an intermediate number of perpendicular angles in fact display characteristics of both icosahedral and face-centered-cubic structures and may be regarded as truly amorphous, as they are not otherwise easily classified. It turns out that this identification of icosahedra is substantially more generous towards them than some other criteria. For example, another reasonable criterion is that icosahedra should have all 12 perimeter particles coordinated with exactly five near neighbors (and cpc clusters should have no such perimeter particles), using the r_{NN} calculated for the inherent structure. Only about one-fifth as many clusters identified in Table V below as icosahedral would qualify with this much more strict criterion; typically, the majority of 12-coordination clusters in any inherent structure possess between zero and five five-coordination perimeter particles. Yet another criterion, employed earlier by the author and that sorts clusters according to the distribution of the pair distances between all the perimeter particles is even more demanding,

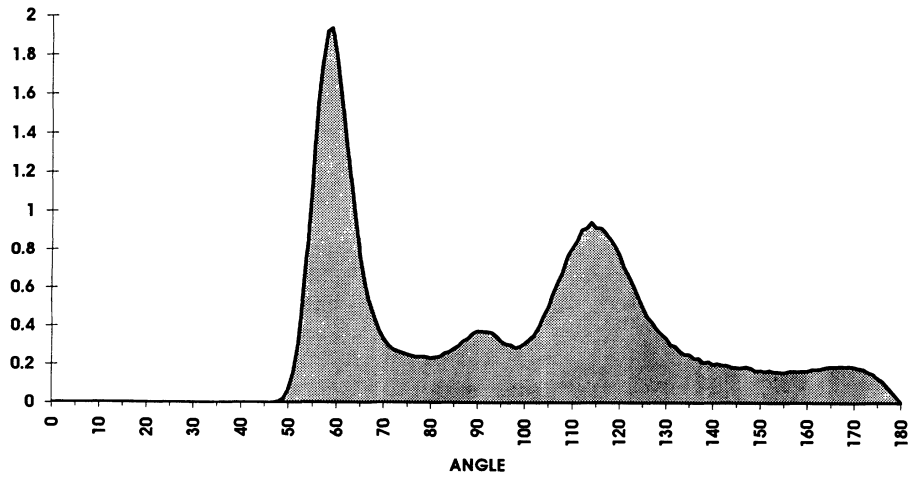

FIG. 9. Angle distribution for 12-coordinated particles in the inherent structure at $n = 1.32$.

TABLE V. Distribution of perpendicular angles among 12-coordinated clusters. The first row shows the density of each of the inherent structures surrounded to two decimal places; see Table II for the densities to four places. The first column shows the number of perpendicular angles. The values 0 and 12 correspond to the ico and cpc clusters, respectively. The * marks the maximum in the distribution for each density. The columns do not add up to 100% in part due to rounding errors and in part due to the neglect here of the statistically insignificant population of clusters with more than 12 perpendicular angles.

Density	1.32	1.40	1.45	1.52	1.57	1.62	1.97
0	2%	3%	5%	5%	4%	4%	2%
1	3%	4%	6%	6%	5%	6%	3%
2	5%	6%	7%	7%	6%	9%	5%
3	8%	8%	10%	9%	8%	12%	9%
4	14%	12%	13%	12%	11%	*17%	12%
5	16%	15%	*16%	*15%	13%	17%	16%
6	*17%	*16%	15%	15%	*15%	14%	*16%
7	14%	14%	12%	12%	14%	10%	13%
8	10%	10%	8%	9%	11%	6%	10%
9	6%	7%	5%	6%	7%	3%	6%
10	3%	4%	2%	2%	3%	1%	4%
11	1%	2%	0.8%	1%	2%	0.4%	3%
12	0.3%	0.7%	0.3%	0.8%	1%	0.1%	2%

for with this criterion, the concentration of icosahedra listed in Table V would fall by at least an order of magnitude.

The distribution of perpendicular angles among the 12-coordination clusters is listed in Table V; a typical distribution (at $n=1.45$) is shown in Fig. 10. Typically, more than half of the clusters contain between four and seven perpendicular angles; fewer than 5% are icosahedral (0 perpendicular angles), and fewer than 1% are cpc (12 perpendicular angles). Inspection of a few of the clusters with six perpendicular angles revealed that the clusters appear icosahedral in one hemisphere, and crystalline in the other.

Inspection of a few cpc clusters suggested that they were strained, or at least compressed, that is, they appeared to correspond to lattices of a higher density than the density of the inherent structure. In order to quantify this observation, the energies of all the 12-coordination clusters (including the 13th central particle) were sorted according to the number of perpendicular angles in the cluster; the results are displayed in Table VI. A comparison was made between the mean energies of the cpc clusters and the energies of the 12-coordination cluster extracted from the fcc lattice of various densities (the energetic differences between the clusters with hcp and fcc lattices, respectively, are small enough to be ignored for the purposes of this comparison). It was determined that the cpc clusters in the inherent structure were slightly compressed relative to the inherent structure. These results are also included in Table VI. The icosahedra also are compressed, which may account for the observation (cf. Table VI) that here the icosahedral clusters possess the highest energies of all the 12-coordination cluster types at every density.

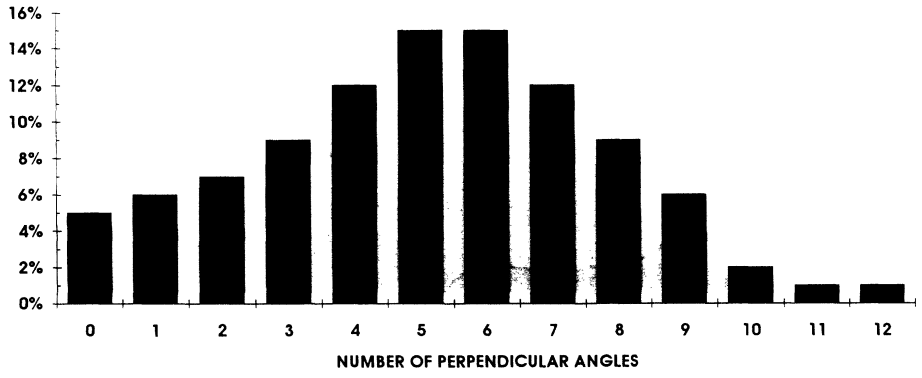

FIG. 10. Distribution of perpendicular angles among the 12-coordinated particles in the inherent structure at $n=1.52$ (see Table V).

TABLE VI. Lattice densities and mean energies of 12-coordinated clusters distributed according to the number of perpendicular angles. The first row shows the density of each of the inherent structures. The second row shows the effective density of cpc clusters (those with 12 perpendicular angles) obtained by matching their energy with that of the fcc cluster with the appropriate lattice parameter. The next 13 rows show the energy of the clusters according to the number of perpendicular angles, respectively. The * marks energy minima for each density. The last row shows the energy of an isolated 13-particle cluster with the fcc structure at the density of the inherent structure, where the density was taken to four decimal places rather than to the two shown above. The lowest energy of an isolated fcc or hcp crystallite of 13 *hx* particles is −36.062 (with lattice parameters corresponding to a density of 0.793); the global energy minimum for a cluster of 13 *hx* particles is −41.802, in an icosahedral cluster with a radius of 1.299 259 6.

Density							
Effective	1.32	1.40	1.45	1.52	1.57	1.62	1.97
cpc density	1.41	1.49	1.55	1.61	1.65	1.71	2.00
0	−15.26	−11.18	−7.32	−1.41	4.09	9.88	78.31
1	−15.67	−11.11	−7.64	−1.66	3.29	9.77	77.48
2	−15.72	−11.44	−7.75	−1.50	3.89	9.69	78.04
3	−15.74	−11.32	−7.83	−1.52	3.97	9.88	77.84
4	−15.88	−11.43	−7.90	−1.60	3.75	9.59	77.15
5	−16.13	−11.66	−7.93	−1.62	3.75	9.74	76.81
6	−16.27	−11.74	−8.08	−1.77	3.65	9.68	76.11
7	−16.49	−11.88	−8.29	−1.69	3.62	9.39	74.80
8	−16.66	−12.03	−8.40	−1.89	3.42	9.19	73.37
9	−16.89	−12.24	−8.57	−2.09	3.40	8.93	71.22
10	−17.12	−12.38	*−8.67	*−2.42	3.09	8.80	66.76
11	−17.06	− 12.40	−8.65	−2.32	2.94	*8.77	64.04
12	*−17.91	*−12.74	−7.90	−1.52	*2.79	9.81	*62.34
fcc lattice	−22.26	−18.25	−15.23	−10.19	−5.81	−0.99	54.88

VII. CONCLUSIONS

One of the lessons learned here is that the usual bulk measures, such as the equation of state, or the usual order parameters, such as the pair distribution function, are inadequate for resolving the details of the local structure of amorphous packings. Even "computer experiments" are difficult to analyze, in spite of the advantages of knowing precisely the coordinates of each particle. These remarks suggest that decisive experimental determinations of the structure of these kind of amorphous substances will be difficult and therefore may not be rapidly forthcoming. On the other hand, as discussed below, a simple theoretical description of these packings also may be far in the future.

The first part of Frank's suggestion for the local structure of amorphous packings,[1] namely, that in the densest packings the local structural motif should be noncrystalline, was well founded and is verified in this work. However, the second part of his argument, namely, that the noncrystalline alternative should be instead icosahedral, fails in the cases considered here. First, icosahedra are always rare. Second, the icosahedra possess the highest potential energy among the 12-coordination clusters, even though they have the lowest energy in isolation. Third, the 12-coordination clusters that do possess the lowest energy are not the most abundant, as a comparison between Tables V and VI reveals. The most common 12-coordination clusters are, with respect to the geometrical attributes considered in Sec. VI above, almost perfectly halfway between the crystal close-packed and icosahedral arrangements. The fact that the most abundant 12-coordination clusters share attributes of both icosahedral and crystalline arrangements also shows how easily both pure theorists and "computer experimentalists" might have oversimplified the picture of the local structure because those looking for either one or the other arrangement would have found evidence to support their case. Finally, the most common 12-coordination clusters do appear to contain at least a hemisphere that is crystalline and therefore could serve as a nucleation site or template. The argument against microcrystallites that is derived from a requirement for an absence of crystal nucleation sites does not succeed here.

These remarks also suggest that a simple theory of the densest amorphous packings is not likely to appear soon, for the local structural motifs cannot be resolved into a simple dichotomy. The last significant theoretical advance on this subject was a mathematical *tour de force,* which nevertheless failed to correctly identify the predominant local structure.[7] Apparently a much larger number of structure types now must be considered by theory. Theory will also require a more accurate approach to untangling the complicated interactions between atoms in a given cluster with the rest of the system, and a more accurate treatment of the entropy of the cluster. In circumstances where everything seems important, theory is often found to fall short; this study apparently provides such a circumstance.

In the case of the lower-density packings, the theoreti-

cal situation may be more promising. In these cases, even the first part of Frank's suggestion fails to describe the dominant local structure for most of this density range, although in retrospect it might have been unreasonable to apply it at all to the lower-coordination packings. Instead, crystalline local order is abundant, except at the very lowest densities. Even a transition is observed between two crystalline types of the same coordination. It is likely that either the continuous random-network models or the dense random-packing models would predict that nearly all the clusters would be like hxg, the noncrystalline icosahedral fragment, which minimizes the isolated cluster. However, Phillips' constraint theory[13–16] apparently does possess the essential ingredients which might provide a prediction for these observations. The constraint theory recognizes that crystalline arrangements might dominate the local order. Furthermore, the idea in constraint theory that the representative crystallite comes from the high-temperature phase might explain the sudden appearance of bcc clusters at densities well below the bulk crystalline hex-bcc transition. Although the phase diagram for the *hx* model has not been elucidated, it is likely that there is a high-temperature bcc phase at densities where the low-temperature crystal phase is simple hexagonal, under constant-volume conditions.[19]

Evidence has been presented for the presence and even dominance of crystalline local order in amorphous quenches of this model liquid. This observation removes the widely accepted explanation for what Hoare[2] calls self-limiting growth, namely, that the local order is noncrystalline (or presents no nucleation sites for crystal growth). What then limits the growth of the crystalline phase in the quench? It is likely that the answer is more complicated than any of the explanations proposed so far.

ACKNOWLEDGMENT

This work was supported through the EG&G Idaho Long-Term Research Initiative in Chemical Sciences under DOE Idaho Operations Office Contract No. DE-AC07-76ID01570.

---

*To whom correspondence should be addressed.

†Present address: Department of Civil Engineering, University of Sydney, New South Wales 2006 Australia.

[1]F. C. Frank, Proc. R. Soc. London, Ser. A **215**, 43 (1952).

[2]M. Hoare, Ann. N.Y. Acad. Sci. **279**, 186 (1976), and references therein.

[3]J. Dixmier and J. F. Sadoc, in *Metallic Glasses,* edited by J. J. Gilmand and H. J. Leamy (American Society for Metals, Metals Park, OH, 1976).

[4]P. J. Steinhardt, D. R. Nelson, and M. Ronchetti, Phys. Rev. B **28**, 784 (1983).

[5]D. R. Nelson, Phys. Rev. B **28**, 5515 (1983).

[6]J. P. Sethna, Phys. Rev. B **31**, 6278 (1985).

[7]S. Sachdev and D. R. Nelson, Phys. Rev. B **32**, 1480 (1985).

[8]T. Ichikawa, Phys. Status Solidi A **19**, 707 (1973).

[9]F. H. Stillinger and R. A. LaViolette, Phys. Rev. B **34**, 5136 (1986).

[10]A. S. Clarke and J. D. Wiley, Phys. Rev. B **38**, 3659 (1988).

[11]R. A. LaViolette, Phys. Rev. B **41**, 8526 (1990).

[12]M. Dzugutov, Phys. Rev. A **46**, R2984 (1992).

[13]J. C. Phillips, J. Non-Cryst. Solids **34**, 153 (1979).

[14]J. C. Phillips, *Solid State Physics* (Academic, New York, 1982), Vol. 37.

[15]J. R. Banavar and J. C. Phillips, Phys. Rev. B **28**, 4716 (1983).

[16]J. C. Phillips, Ann. N.Y. Acad. Sci. **484**, 271 (1986).

[17]J. O. Hirschfelder, C. F. Curtiss, and R. B. Bird, *Molecular Theory of Gases and Liquids* (Wiley, New York, 1954).

[18]R. A. LaViolette and F. H. Stillinger, J. Chem. Phys. **82**, 3335 (1985).

[19]The constant-pressure transitions for the zero-temperature crystal may be different: apparently only a hex-fcc transition remains. However, the constant-volume transitions are relevant here because the packings are quenched from the liquid at constant volume.

[20]J. Z. Hu and I. L. Spain, Solid State Commun. **51**, 263 (1984).

[21]C. W. Gear, *Numerical Initial-Value Problems in Ordinary Differential Equations* (Prentice-Hall, Englewood Cliffs, NJ, 1971).

[22]L. C. Kaufmann, MINOP, AT&T Bell Laboratories (unpublished).

[23]F. H. Stillinger and T. A. Weber, Science **225**, 983 (1984).

[24]F. H. Stillinger and R. A. LaViolette, J. Chem. Phys. **83**, 6413 (1985).

[25]W. H. Press, S. A. Teukolsky, W. T. Vetterling, and B. P. Flannery, *Numerical Recipies in Fortran,* 2nd ed. (Cambridge University Press, London, 1992).

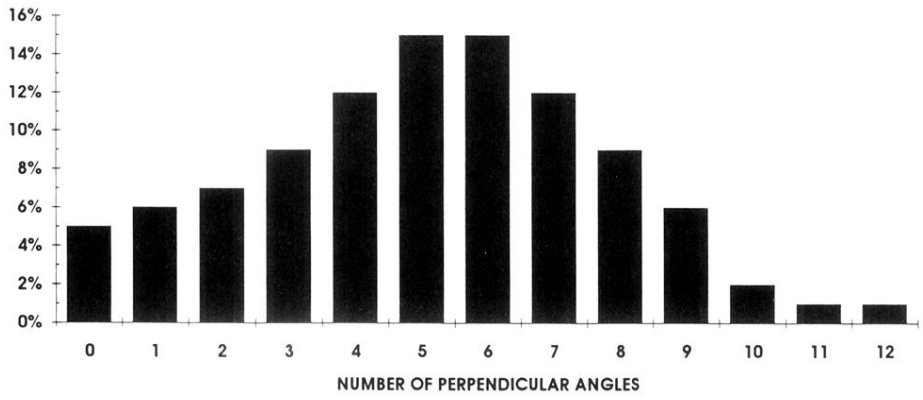

FIG. 10. Distribution of perpendicular angles among the 12-coordinated particles in the inherent structure at $n=1.52$ (see Table V).

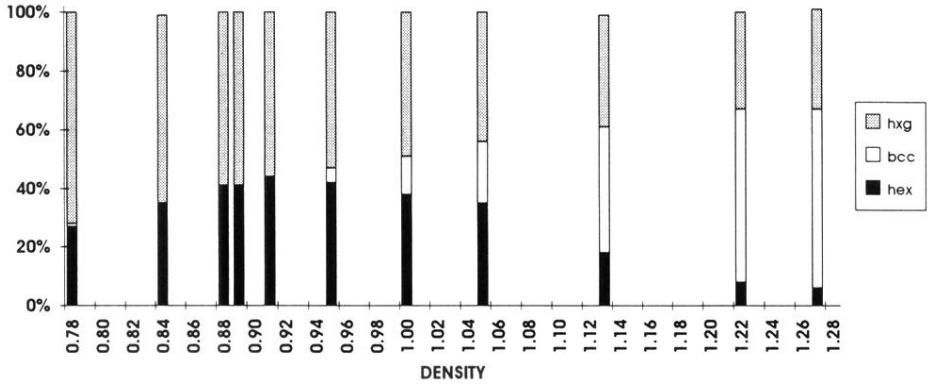

FIG. 8. Relative population of the three eight-coordination structure types in the inherent structure for various densities (see Table IV).

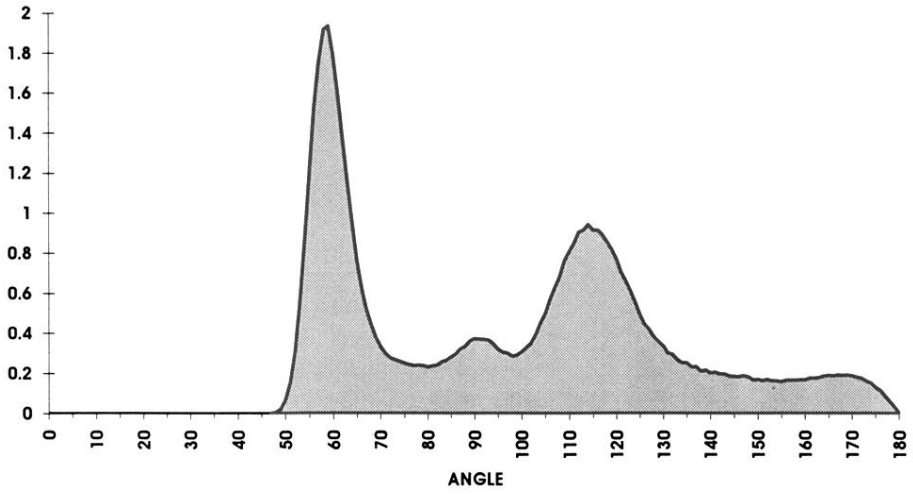

FIG. 9. Angle distribution for 12-coordinated particles in the inherent structure at $n = 1.32$.